

Signals for Lorentz violation in gravitational waves

Matthew Mewes

Physics Department, California Polytechnic State University, San Luis Obispo, California 93407, USA

Lorentz violations in gravitational waves are investigated. Plane-wave solutions for arbitrary gauge-invariant violations in linearized gravity are constructed. Signatures of Lorentz violation include dispersion, birefringence, and anisotropies. Modifications to waves from coalescing compact binaries and to strain signals in gravitational-wave detectors are derived.

I. INTRODUCTION

The growing catalog of gravitational-wave observations [1–6] offers new opportunities for tests of fundamental physics. Lorentz invariance is a feature of both Einstein’s general relativity and the standard model of particle physics, so any breaking of this symmetry would signal new physics [7–10] potentially rooted in quantum gravity [11]. Because of the large propagation distances, gravitational waves produced in binary mergers are particularly sensitive to defects in relativity, enabling new precision tests of Lorentz invariance in gravity [3, 12–21].

Lorentz invariance is the combination of both rotation symmetry and boost symmetry, so Lorentz violations generally produce unexpected directional and velocity dependences. One consequence is modified kinematics for particles and waves. However, to fully characterize the effects of Lorentz violation one needs a complete dynamical model of the system. A theoretical framework known as the Standard-Model Extension (SME) characterizes general violations of Lorentz and CPT invariance in both general relativity and the standard model at attainable energies [9, 10]. A Lorentz-violating term in the SME action is formed from the contraction of a conventional tensor operator with a tensor coefficient for Lorentz violation. The terms are classified according to the mass dimension d of the operator in natural units with $\hbar = c = 1$ [22, 23]. It is generally assumed that higher- d terms represent higher-order corrections to conventional physics.

While particle sectors of the SME have received intense scrutiny over the last two decades [8], fewer searches for Lorentz violation in gravity have been performed. Tests of Lorentz violation in gravitational waves include searches for birefringence [12] and dispersion [16]. Other tests of Lorentz invariance in the SME gravity sector include those involving gravitational Čerenkov radiation [21], atomic interferometers [24], superconducting gravimeters [25], orbital dynamics [26–29], short-range-gravity experiments [30, 31], comagnetometers [32], nuclear binding energy [33], and very-long-baseline interferometry [34]. The SME also serves as the foundation for a number of theoretical studies of Lorentz violation in gravity [35–40].

The development of the gravity sector of the SME has progressed along several parallel lines, each corresponding to a different limit of the theory. The most general extension describes violations in gravity and particles, including gravitational couplings to standard-model fields

[10]. It is based on Riemann-Cartan geometry, where the vierbein e_μ^a is the gravitational field. One can then focus on matter-gravity couplings [35] or on the pure-gravity sector [36]. The pure-gravity limit assumes Riemannian geometry. The usual Einstein-Hilbert action is then augmented by all possible coordinate-independent terms involving the metric $g_{\mu\nu}$.

The above construction produces an effective field theory that encompasses all realistic violations of Lorentz invariance in gravity, whether they are explicit or dynamically generated [37]. However, the difficulties of working in a nonlinear theory like general relativity are only exacerbated by the inclusion by Lorentz violation, encumbering systematic studies. We can avoid many of the complications by working at the level of linearized gravity [41]. In this limit of the SME, one posits that gravity is suitably weak and expands the metric $g_{\mu\nu} = \eta_{\mu\nu} + h_{\mu\nu}$ about the constant Minkowski metric $\eta_{\mu\nu}$. The action is constructed from all possible Lorentz-invariant and Lorentz-violating terms quadratic in the metric perturbation $h_{\mu\nu}$.

The full linearized-gravity extension is constructed in Refs. [12, 39]. It takes the form of an effective field theory in flat spacetime, making its development and application comparatively simple. The action contains the linearized limit of all Lorentz and diffeomorphism violations in general relativity, including those that violate the usual gauge invariance, $h_{\mu\nu} \rightarrow h_{\mu\nu} + \partial_{(\mu}\xi_{\nu)}$. Work involving the linear extension includes studies of gravitational-wave dispersion relations for gauge-invariant [12] and gauge-breaking violations [39] and studies of Lorentz violation in newtonian gravity [40].

Some of the tightest constraints on Lorentz violation in any sector come from observations of radiation from astrophysical sources, where tiny modifications to the dynamics can accumulate over cosmological times. For example, searches for photon dispersion [42–44], photon birefringence [43–45], and unconventional Čerenkov radiation [46, 47] have all placed tight limits on particle-sector Lorentz violation.

In gravitational waves, dispersion causes a deformation of the waveform, and birefringence causes changes in the polarization. Both will distort the strain signal measured by gravitational-wave observatories. This paper characterizes dispersion and birefringence due to Lorentz violation and the effects of Lorentz violation on gravitational waves produced in the coalescence of compact binaries.

We restrict attention to the gauge-invariant linearized-gravity sector of the SME [12]. We find that this limit

produces two independent modes for propagation with differing phase velocities and conventional polarizations at zeroth order in Lorentz violation. Note, however, that the full SME includes gauge-breaking terms, which are expected to produce effects beyond those discussed here. For example, new exotic modes may propagate that could be detected in observations of gravitational waves [5, 48].

Throughout this work, we adopt units with $c = 1$, but explicitly include Newton's constant G_N . Setting $G_N = 1$ yields geometrized units. Alternatively, setting $\hbar = 1$ gives natural units and $G_N = 1/M_{\text{Pl}}^2$, where M_{Pl} is the Planck mass. Spacetime indices are raised and lowered using the Minkowski metric with $(-, +, +, +)$ signature.

This paper is organized as follows. Section II examines gravitational plane waves in gauge-invariant linearized gravity with Lorentz violation. In Sec. III, we consider waves created in binary mergers and derive the modified detector strain including the effects of Lorentz violation during propagation. Section IV provides a summary and some concluding remarks. The effects of Lorentz violation on gravitational Stokes parameters are discussed in the Appendix.

II. GRAVITATIONAL WAVES

In this section, we find plane-wave solutions for gravitational waves in the presence of Lorentz violation. We begin by first reviewing the gauge-invariant linearized-gravity sector of the SME. We then derive the leading-order dispersion relation and the polarizations of the propagating modes. The effects on waves that have traveled astrophysical distances are explored, and several special cases are discussed.

A. Basic theory

The lagrangian for the gauge-invariant linearized-gravity sector of the SME consists of all possible terms quadratic in $h_{\mu\nu}$, including arbitrary numbers of derivatives of $h_{\mu\nu}$. It contains the usual linearized Einstein-Hilbert lagrangian and an infinite series of Lorentz-invariant and Lorentz-violating terms. It can be written in the compact form [12]

$$\mathcal{L} = \frac{1}{4}\epsilon^{\mu\rho\alpha\kappa}\epsilon^{\nu\sigma\beta\lambda}\eta_{\kappa\lambda}h_{\mu\nu}\partial_\alpha\partial_\beta h_{\rho\sigma} + \frac{1}{4}h_{\mu\nu}(\hat{s}^{\mu\nu\rho\sigma} + \hat{q}^{\mu\nu\rho\sigma} + \hat{k}^{\mu\nu\rho\sigma})h_{\rho\sigma}. \quad (1)$$

Each term is invariant under the usual gauge transformation $h_{\mu\nu} \rightarrow h_{\mu\nu} + \partial_{(\mu}\xi_{\nu)}$ up to a total derivative. The first line in Eq. (1) is the conventional lagrangian and generates the usual linearized Einstein tensor $G^{\mu\nu} = -\frac{1}{2}\eta_{\rho\sigma}\epsilon^{\mu\rho\alpha\kappa}\epsilon^{\nu\sigma\beta\lambda}\partial_\alpha\partial_\beta h_{\kappa\lambda}$.

The last term in Eq. (1) contains the Lorentz-violating modifications. It naturally splits into three different

classes of violations, corresponding to the operators

$$\begin{aligned} \hat{s}^{\mu\nu\rho\sigma} &= \sum s^{(d)\mu\rho\alpha_1\nu\sigma\alpha_2\dots\alpha_{d-2}}\partial_{\alpha_1}\dots\partial_{\alpha_{d-2}}, \\ \hat{q}^{\mu\nu\rho\sigma} &= \sum q^{(d)\mu\rho\alpha_1\nu\sigma\alpha_2\dots\alpha_{d-2}}\partial_{\alpha_1}\dots\partial_{\alpha_{d-2}}, \\ \hat{k}^{\mu\nu\rho\sigma} &= \sum k^{(d)\mu\alpha_1\nu\alpha_2\rho\alpha_3\sigma\alpha_4\dots\alpha_{d-2}}\partial_{\alpha_1}\dots\partial_{\alpha_{d-2}}. \end{aligned} \quad (2)$$

The tensor coefficients in these expansions control the Lorentz violation. Each has different symmetries, which are summarized in Table 1 of Ref. [12]. The s - and k -type violations are CPT even, while q -type violations break CPT invariance in addition to Lorentz invariance. For particles, CPT breaking typically leads to different properties for particles and antiparticles. For gravitational waves, CPT violation breaks the degeneracy between left- and right-handed polarizations. The sums in Eq. (2) are over even $d \geq 4$ for s -type violations, odd $d \geq 5$ for q -type, and even $d \geq 6$ for k -type.

The equations of motion for Eq. (1) can be written in the form

$$0 = G^{\mu\nu} + \delta M^{\mu\nu\rho\sigma} h_{\rho\sigma}, \quad (3)$$

where the tensor operator

$$\begin{aligned} \delta M^{\mu\nu\rho\sigma} &= -\frac{1}{4}(\hat{s}^{\mu\rho\nu\sigma} + \hat{s}^{\mu\sigma\nu\rho}) - \frac{1}{2}\hat{k}^{\mu\nu\rho\sigma} \\ &\quad - \frac{1}{8}(\hat{q}^{\mu\rho\nu\sigma} + \hat{q}^{\nu\rho\mu\sigma} + \hat{q}^{\mu\sigma\nu\rho} + \hat{q}^{\nu\sigma\mu\rho}) \end{aligned} \quad (4)$$

contains the unconventional parts. This operator is symmetric in the first pair of indices and the last pair of indices. The CPT-even part of $\delta M^{\mu\nu\rho\sigma}$ is symmetric under interchange of the first and last pair of indices and involves an even number of derivatives. The CPT-odd part is antisymmetric under interchange of the pairs of indices and contains an odd number of derivatives. Consequently, $\delta M^{\mu\nu\rho\sigma}$ is a hermitian operator acting on the space of symmetric rank-2 tensors.

B. Eigenmodes

We next derive leading-order plane-wave solutions of the equations of motion. A fourier transform converts $\partial_\alpha \rightarrow ip_\alpha$ and Eq. (3) to a p -dependent matrix equation. The operators $\hat{s}^{\mu\rho\nu\sigma}$, $\hat{q}^{\mu\rho\nu\sigma}$, and $\hat{k}^{\mu\nu\rho\sigma}$ are now interpreted as functions of p_α . Solving the p -space equations of motion gives plane-wave solutions with wave vector $p^\alpha = (\omega; \vec{p})$. To handle both positive and negative frequencies, it is useful to write $\vec{p} = \omega\hat{v}/v$. The unit vector $\hat{v} = \text{sgn}(\omega)\vec{p}/|\vec{p}|$ points in the direction of propagation, and $v = |\omega|/|\vec{p}|$ is the phase velocity. Note that \hat{v} points in the direction of \vec{p} for positive frequencies and opposite to \vec{p} for negative frequencies.

In the usual case, one normally starts in a Hilbert gauge by imposing the Lorenz condition $p_\nu \bar{h}^{\mu\nu} = 0$. The Einstein equation then reads $G^{\mu\nu} = \frac{1}{2}p^2 \bar{h}^{\mu\nu} = 0$, giving the dispersion relation $p^2 = 0$. On shell, you can choose a gauge that is temporal ($h^{0\mu} = 0$), transverse ($h^{jk}p^k = 0$),

and traceless ($h^{jj} = 0$), leading to the transverse traceless gauge. Two degrees of freedom remain, giving two degenerate polarizations.

In the Lorentz-violating case, where the on-shell p_α is no longer light-like, we cannot necessarily impose all of the above gauge conditions simultaneously. It is convenient, however, to work in the temporal gauge. The other gauge conditions may or may not be satisfied on shell. An advantage of the temporal gauge is that coordinates for free nonrelativistic test masses are inertial, since $\partial_t^i x^j \approx -\Gamma_{00}^j$.

It is also useful to work in a helicity basis with basis vectors [22]

$$\begin{aligned}\hat{e}_r &= \hat{e}^r = \hat{v} = (\sin\theta \cos\phi, \sin\theta \sin\phi, \cos\theta), \\ \hat{e}_\pm &= \hat{e}^\mp = \frac{1}{\sqrt{2}}(\hat{e}_\theta \pm i\hat{e}_\phi).\end{aligned}\quad (5)$$

The propagation vector \hat{v} defines the ‘‘radial’’ direction, and \hat{e}_θ and \hat{e}_ϕ are the usual unit vectors associated with spherical-coordinate angles θ and ϕ . The complex helicity vectors \hat{e}_\pm span the transverse subspace.

In the temporal gauge, only the spatial parts of $h_{\mu\nu}$ are nonzero, which we write as $\overleftrightarrow{h} = h^{ab}\hat{e}_a \otimes \hat{e}_b$ in terms of helicity-basis components $h^{ab} = \hat{e}^a \cdot \overleftrightarrow{h} \cdot \hat{e}^b$. Note that raising and lowering spatial indices in the helicity basis is done using the skew-diagonal helicity metric $\eta_{ab} = \eta^{ab} = \hat{e}_a \cdot \hat{e}_b$. The result is that raising or lowering helicity-basis indices changes \pm to \mp . For example, $G^{r+} = G_{r-}$.

The ten helicity components of the p -space Einstein tensor can be written in terms of the six components of the temporal-gauge \overleftrightarrow{h} . The unconventional 0-helicity components are given by $G^{rr} = vG^{0r} = v^2G^{00} = \omega^2 h^{+-}$ and $G^{+-} = \frac{\omega^2}{2}h^{rr} - \frac{v^2}{2}h^{+-}$. The ± 1 -helicity components obey $G^{r\pm} = vG^{0\pm} = -\frac{\omega^2}{2}h^{r\pm}$. The transverse ± 2 -helicity components give $G^{\pm\pm} = \frac{v^2}{2}h^{\pm\pm}$. In the usual case, where $G^{\mu\nu} = 0$ and $p^2 = 0$, only the $h^{\pm\pm}$ components can be nonzero, giving an \overleftrightarrow{h} that is transverse and traceless. In the Lorentz-violating case, we can use the above relations to construct perturbative solutions.

Assuming the 0-helicity and ± 1 -helicity components of \overleftrightarrow{h} are small, the leading-order ± 2 -helicity components $h^{\pm\pm}$ satisfy the matrix equation

$$\begin{pmatrix} p^2 + 2\delta M^{++++} & 2\delta M^{++++} \\ 2\delta M^{----} & p^2 + 2\delta M^{----} \end{pmatrix} \begin{pmatrix} h_{(+2)} \\ h_{(-2)} \end{pmatrix} = 0, \quad (6)$$

where we denote

$$h_{(\pm 2)} = h^{\pm\pm}. \quad (7)$$

After solving for the leading-order $h_{(\pm 2)}$, we can use them and the modified Einstein equation (3) to perturbatively solve for higher-order corrections to the polarization. This procedure leads to a temporal-gauge $h^{\mu\nu}$ that differs from a conventional $h^{\mu\nu}$ by corrections that are suppressed by coefficients for Lorentz violation. Note

that the result is neither transverse nor traceless. However, the unconventional parts are likely to be too small to be directly observable. Therefore, the dominant effect of Lorentz violation on the polarization is a possible breaking of the usual degeneracy between the two polarizations, resulting in birefringence.

Each of the matrix elements in Eq. (6) has definite helicity. The diagonal elements of the square matrix have zero helicity, while the off-diagonal elements have helicity ± 4 , coupling the right-handed $h_{(+2)}$ and left-handed $h_{(-2)}$ polarizations. The trace element preserves the usual degeneracy between the two polarizations, motivating the following definition

$$\begin{aligned}\zeta^0 &= -\frac{1}{2\omega^2}(\delta M^{++--} + \delta M^{--++}) \\ &= \frac{1}{2\omega^2}(\hat{s}^{+-+-} + \hat{k}^{+--+}).\end{aligned}\quad (8)$$

We expect the remaining parts to break the degeneracy, giving birefringence. We define these as

$$\begin{aligned}\zeta_{(0)} &= \frac{1}{2\omega^2}(\delta M^{++++} - \delta M^{----}) = -\frac{1}{2\omega^2}\hat{q}^{++++}, \\ \zeta_{(\pm 4)} &= \frac{1}{2\omega^2}\delta M^{\pm\pm\pm\pm} = -\frac{1}{2\omega^2}\hat{k}^{\pm\pm\pm\pm}.\end{aligned}\quad (9)$$

The combinations ζ^0 and $\zeta_{(0)}$ are real and have zero helicity, while $\zeta_{(\pm 4)}$ have helicity ± 4 and obey $\zeta_{(\pm 4)}^* = \zeta_{(\mp 4)}$.

In this work the ζ functions are found by fixing the gauge and working in the helicity basis. Note, however, that covariant versions of these functions and the dispersion relation are derived in Ref. [12] without gauge fixing using the methods discussed in Ref. [39].

As discussed in the Appendix, the p -dependent coefficient combinations ζ^0 , $\zeta_{(0)}$, $\zeta_{(+4)}$, $\zeta_{(-4)}$ can be interpreted as conveniently normalized Stokes parameters for the faster propagating mode. They are functions of the frequency ω and the wave vector \vec{p} . However, when evaluating the ζ functions, we can assume the usual energy-momentum relation and take $\vec{p} = \omega\hat{v}$ at leading order. We then get functions that depend on the frequency ω and propagation direction \hat{v} . They can be written as

$$\begin{aligned}\zeta^0 &= \sum_d \omega^{d-4} \zeta^{(d)0}(\hat{v}), \\ \zeta_{(\pm 4)} &= \sum_d \omega^{d-4} \zeta_{(\pm 4)}^{(d)}(\hat{v}), \\ \zeta_{(0)} &= \sum_d \omega^{d-4} \zeta_{(0)}^{(d)}(\hat{v}),\end{aligned}\quad (10)$$

separating the frequency and direction dependences.

The direction-dependent factors can be expanded in spin-weighted spherical harmonics ${}_s Y_{jm}$. Spin weight is the opposite of helicity [22], so the expansions take the form [12]

$$\begin{aligned}\zeta^{(d)0}(\hat{v}) &= \sum_{jm} (-1)^j {}_0 Y_{jm}(\hat{v}) k_{(I)jm}^{(d)}, \\ \zeta_{(\pm 4)}^{(d)}(\hat{v}) &= \sum_{jm} (-1)^j {}_{\mp 4} Y_{jm}(\hat{v}) (k_{(E)jm}^{(d)} \pm i k_{(B)jm}^{(d)}), \\ \zeta_{(0)}^{(d)}(\hat{v}) &= \sum_{jm} (-1)^j {}_0 Y_{jm}(\hat{v}) k_{(V)jm}^{(d)}.\end{aligned}\quad (11)$$

| Coefficient | d | j | Number |
|-------------------|----------------|--------------------|----------------|
| $k_{(I)jm}^{(d)}$ | even, ≥ 4 | $0, 1, \dots, d-2$ | $(d-1)^2$ |
| $k_{(V)jm}^{(d)}$ | odd, ≥ 5 | $0, 1, \dots, d-2$ | $(d-1)^2$ |
| $k_{(E)jm}^{(d)}$ | even, ≥ 6 | $4, 5, \dots, d-2$ | $(d-1)^2 - 16$ |
| $k_{(B)jm}^{(d)}$ | even, ≥ 6 | $4, 5, \dots, d-2$ | $(d-1)^2 - 16$ |

TABLE I: Summary of the spherical coefficients for Lorentz violation [12]. The second and third columns give the ranges for the dimension index d and angular-momentum index j . The m index obeys the usual relation $-j \leq m \leq j$. The last column gives the total number of independent coefficients for each d . Each set of coefficients obeys the complex-conjugation relation $k_{jm}^{(d)*} = (-1)^m k_{j(-m)}^{(d)}$.

The spherical coefficients for Lorentz violation $k_{(I)jm}^{(d)}$, $k_{(V)jm}^{(d)}$, $k_{(E)jm}^{(d)}$ and $k_{(B)jm}^{(d)}$ are linear combinations of the underlying tensor coefficients in Eq. (2). The connection places limits on the angular momentum indices j and m for each dimension d . These limits, along with the coefficient count, are given in Table I. The spherical coefficients for Lorentz violation have mass dimension $4-d$ in units with $\hbar = 1$. In geometrized units, they have length dimension $d-4$. Note that $(-1)^j {}_s Y_{jm}(\hat{v}) = -{}_s Y_{jm}(-\hat{v})$, which is convenient in astrophysical tests where $-\hat{v}$ gives the location of the source.

Different physical systems access different linear combinations of the fundamental coefficients [40]. The spherical coefficients in Eq. (11) represent the subset affecting gravitational waves at leading order. Note, however, that a given point source with fixed observed \hat{v} can at most measure the four linear combinations of spherical coefficients given in Eq. (11). Different sources with different \hat{v} will access different linear combinations. One can in principle disentangle the numerous spherical coefficients for Lorentz violation at any dimension d by combining data from multiple sources at different locations on the sky.

Nontrivial solutions to Eq. (6) exist when the determinant of the 2×2 matrix vanishes. This gives the dispersion relation

$$p^2 = 2\omega^2(\zeta^0 \mp |\zeta|) , \quad (12)$$

where we define

$$|\zeta| = \sqrt{|\zeta_{(+4)}|^2 + |\zeta_{(0)}|^2} . \quad (13)$$

Solving for the frequency, the dispersion relation can be written as $|\omega| = (1 - \zeta^0 \pm |\zeta|)|\vec{p}|$, giving phase velocities

$$v_{\pm} = 1 - \zeta^0 \pm |\zeta| . \quad (14)$$

The usual degeneracy between the polarizations is broken when $|\zeta| \neq 0$, as expected, and the two modes propagate at different speeds. The top sign in these expressions corresponds to the fast mode, and the bottom sign gives the slow mode.

To find the polarization of each mode, we solve Eq. (6) on shell. The result can be written in terms of two angles ϑ and φ that completely characterize the polarizations of the modes. They are defined through

$$\sin \vartheta = \frac{|\zeta_{(+4)}|}{|\zeta|} , \quad \cos \vartheta = \frac{\zeta_{(0)}}{|\zeta|} , \quad e^{\mp i\varphi} = \frac{\zeta_{(\pm 4)}}{|\zeta_{(+4)}|} . \quad (15)$$

We then find that the fast mode has normalized polarization

$$\begin{pmatrix} h_{(+2)} \\ h_{(-2)} \end{pmatrix}_{\text{fast}} = \begin{pmatrix} \cos \frac{\vartheta}{2} e^{-i\varphi/2} \\ \sin \frac{\vartheta}{2} e^{i\varphi/2} \end{pmatrix} , \quad (16)$$

while the polarization of the slow mode can be written

$$\begin{pmatrix} h_{(+2)} \\ h_{(-2)} \end{pmatrix}_{\text{slow}} = \begin{pmatrix} -\sin \frac{\vartheta}{2} e^{-i\varphi/2} \\ \cos \frac{\vartheta}{2} e^{i\varphi/2} \end{pmatrix} . \quad (17)$$

A general polarization is a linear combination of the two eigenmodes. The unitary transformation

$$\begin{pmatrix} h_{(+2)} \\ h_{(-2)} \end{pmatrix} = \begin{pmatrix} \cos \frac{\vartheta}{2} e^{-i\varphi/2} & -\sin \frac{\vartheta}{2} e^{-i\varphi/2} \\ \sin \frac{\vartheta}{2} e^{i\varphi/2} & \cos \frac{\vartheta}{2} e^{i\varphi/2} \end{pmatrix} \begin{pmatrix} h_{(f)} \\ h_{(s)} \end{pmatrix} \quad (18)$$

relates the helicity components $h_{(\pm 2)}$ of an arbitrary polarization to its fast-mode component $h_{(f)}$ and its slow-mode component $h_{(s)}$.

Combined with the dispersion relation (12), the above polarizations describe the leading-order effects in gravitational waves for any gauge-invariant extension to linearized gravity, including all possible Lorentz-violating and Lorentz-invariant modifications.

C. Dispersion and birefringence

The unconventional parts of the phase velocity lead to a gradual shift in phase as the wave propagates. Consider, for example, a simple plane wave in flat space-time that has propagated a distance l . For a deformed phase velocity $v = 1 + \delta v$, we get $h(t) \sim e^{-i\omega(t-l/v)} \approx e^{-i\omega\delta v l} e^{-i\omega(t-l)}$, shifting the phase by $\omega\delta v l$.

For cosmological sources in an expanding universe, the redshift of the frequency can be accounted for by considering an infinitesimal change in the phase, $d\psi = d\psi_0 + \omega\delta v dl$. Integrating from the source to the observer, the first part gives the conventional phase. The second part gives the Lorentz-violating contribution, $\delta\psi_{\pm} = \int dl \omega(-\zeta^0 \pm |\zeta|)$, for the fast and slow modes. At zeroth order, the wave propagates at $v = 1$, so we can replace the distance interval dl with the propagation time $dt = -dz/(1+z)/H(z)$, where $H(z)$ is the Hubble expansion rate at redshift z . The accumulated Lorentz-violating phase is then given by

$$\delta\psi_{\pm} = \omega \int_0^z dz \frac{-\zeta^0 \pm |\zeta|}{H(z)} = -\delta \pm \beta , \quad (19)$$

where ω is the observed frequency. The common phase δ is independent of polarization and leads to dispersion but no birefringence. The birefringent phase β is the polarization dependent, causing the net polarization to evolve as the wave propagates. For fixed dimension d , we can write the phases as

$$\delta = \omega^{d-3} \tau \zeta^{(d)0}, \quad \beta = \omega^{d-3} \tau |\zeta^{(d)}|, \quad (20)$$

where

$$\tau = \int_0^z \frac{(1+z)^{d-4}}{H(z)} dz \quad (21)$$

is an effective d -dependent propagation time that accounts for the redshift in ω during propagation.

As the wave propagates, the phase of the fast and slow components shifts relative to the conventional case, leading to observed components $h_{(f,s)} = e^{i\delta \mp i\beta} h_{(f,s)}^{\text{LI}}$, where $h_{(f,s)}^{\text{LI}}$ is the Lorentz invariant limit. Using Eq. (18), we transform this result to the helicity basis, giving

$$h_{(\pm 2)} = e^{i\delta} (\cos \beta \mp i \cos \vartheta \sin \beta) h_{(\pm 2)}^{\text{LI}} - i e^{i\delta} \sin \vartheta e^{\mp i\varphi} \sin \beta h_{(\mp 2)}^{\text{LI}}. \quad (22)$$

We can also write this in terms of standard ‘‘plus’’ and ‘‘cross’’ linear polarizations, defined as $h_{(+)} = h^{\theta\theta} = -h^{\phi\phi}$ and $h_{(\times)} = h^{\theta\phi} = h^{\phi\theta}$. These are related to the helicity components through

$$h_{(\pm 2)} = h_{(+)} \mp i h_{(\times)}. \quad (23)$$

The changes to the linear polarizations are given by

$$\begin{aligned} h_{(+)} &= e^{i\delta} (\cos \beta - i \sin \vartheta \cos \varphi \sin \beta) h_{(+)}^{\text{LI}} \\ &\quad - e^{i\delta} (\cos \vartheta + i \sin \vartheta \sin \varphi) \sin \beta h_{(\times)}^{\text{LI}}, \\ h_{(\times)} &= e^{i\delta} (\cos \beta + i \sin \vartheta \cos \varphi \sin \beta) h_{(\times)}^{\text{LI}} \\ &\quad + e^{i\delta} (\cos \vartheta - i \sin \vartheta \sin \varphi) \sin \beta h_{(+)}^{\text{LI}}. \end{aligned} \quad (24)$$

Equations (22) and (24) give the predicted effects for general modifications to linearized gravity. They provide a map between the modified theory and the conventional limit and incorporate dispersive changes in phase and changes in polarization due to birefringence.

While the above applies to general cases, one simplifying strategy is to consider various special limits. The three main classes of Lorentz violation in gravitational waves are nonbirefringent violations, CPT-odd birefringent violations, and CPT-even birefringent violations. We briefly consider each of these in turn.

Nonbirefringent violations. The CPT-even $k_{(I)jm}^{(d)}$ coefficients are responsible for nonbirefringent Lorentz violations and exist for even $d \geq 4$. They generally produce a frequency-dependent phase velocity producing dispersion. Note, however, that the $d = 4$ case gives a phase velocity that depends on direction but is frequency independent. Consequently, only $d \geq 6$ violations produce

dispersion. In this limit, the birefringent phase β vanishes, and Eqs. (22) and (24) reduce to $h_{(\cdot)} = e^{i\delta} h_{(\cdot)}^{\text{LI}}$ for all polarizations, giving a change in phase but no change in polarization.

CPT-odd birefringence. The $k_{(V)jm}^{(d)}$ coefficients give both dispersion and birefringence and exist for odd $d \geq 5$. Setting all other coefficients to zero, we find that the eigenmodes are circularly polarized. We get $\vartheta = 0$ when the right-handed polarization $h_{(+2)}$ is faster and $\vartheta = \pi$ when the left-handed polarization $h_{(-2)}$ is faster. In both cases, the circular polarizations acquire a simple phase shift, $h_{(\pm 2)} = h_{(\pm 2)}^{\text{LI}} e^{\mp i\delta\psi}$, where $\delta\psi = \omega^{d-3} \tau \zeta_{(0)}^{(d)}$. The shift in relative phase between the two circular polarizations causes a rotation of the linear polarizations:

$$\begin{pmatrix} h_{(+)} \\ h_{(\times)} \end{pmatrix} = \begin{pmatrix} \cos \delta\psi & -\sin \delta\psi \\ \sin \delta\psi & \cos \delta\psi \end{pmatrix} \begin{pmatrix} h_{(+)}^{\text{LI}} \\ h_{(\times)}^{\text{LI}} \end{pmatrix}. \quad (25)$$

This corresponds to a simple rotation of \hat{h} about \hat{v} by angle $\delta\psi/2$, leaving the degree of linear and circular polarization unchanged. Note that the polarization will remain fixed if the wave is produced in one of the circularly polarized eigenmodes, but frequency dependence in the phase velocity still produces dispersion.

CPT-even birefringence. The $k_{(E)jm}^{(d)}$ and $k_{(B)jm}^{(d)}$ coefficients also give dispersion and birefringence, but exist for even $d \geq 6$. The changes in the wave can be found by setting $\delta = 0$ and $\vartheta = \pi/2$ in Eqs. (22) and (24). The result is more complicated in this case because the eigenmodes are linearly polarized at polarization angles $\varphi/4$ and $\varphi/4 + \pi/4$. Only linearly polarized waves at one of these angles will maintain constant polarization. All waves will experience dispersion due to the frequency-dependent phase velocities.

The effects of birefringence in the CPT-even case and more general cases can be made more transparent by considering the gravitational Stokes parameters, as discussed in the Appendix. In general, birefringence produces a simple rotation of the Stokes vector for the wave about the Stokes vector for the faster eigenmode, which can have any elliptical polarization.

Dimension $d = 4$ violations do not affect chirp observations since they are nondispersive and nonbirefringent. In this case, the phase and group velocities acquire the same frequency- and polarization-independent shift

$$\delta v = \sum (-1)^{j+1} {}_0Y_{jm}(\hat{v}) k_{(I)jm}^{(4)}. \quad (26)$$

While this doesn’t affect chirp signals, it can be tested through time-of-flight comparisons with photons [18, 19]. For example, assuming a common origin for GW170817 and GRB 170817A, Ref. [19] places limits on the difference between the speed of gravity and the speed of light. The result can be translated to a constraint on a combi-

nation of spherical SME coefficients:

$$-3 \times 10^{-15} \leq \sum_{jm} {}_0Y_{jk}(\hat{n}) (c_{(I)jm}^{(4)} - k_{(I)jm}^{(4)}) \leq 7 \times 10^{-16}, \quad (27)$$

where $c_{(I)jm}^{(4)}$ are photon-sector coefficients for Lorentz violation. Here we assume negligible birefringence in photons [45]. Using the location of the optical counterpart [49], the source location $\hat{n} = -\hat{v}$ has angles $\{\theta_{\hat{n}}, \phi_{\hat{n}}\} \simeq \{113^\circ, 197^\circ\}$ in the Sun-centered frame used in tests involving the SME. Restricting attention to the isotropic limit, the shift in the speed of gravity reduces to $\delta v = -\sqrt{1/4\pi} k_{(I)00}^{(4)}$. Assuming isotropy in photons as well, the constraint above gives

$$-11 \times 10^{-15} \lesssim c_{(I)00}^{(4)} - k_{(I)00}^{(4)} \lesssim 25 \times 10^{-16}. \quad (28)$$

III. BINARY COALESCENCE

The goal of this section is to apply the above results to coalescing binaries in order to characterize the signatures of Lorentz violation in chirp signals. We begin by reviewing conventional mergers in the quadrupole approximation, which describes the dominate expected features of the emitted gravitational waves in the Lorentz-invariant case. We then calculate the modifications due to Lorentz violation. General expressions for Earth-incident gravitational waves and detector strains are found in terms of coefficients for Lorentz violation in the standard Sun-centered celestial equatorial reference frame used in Lorentz tests involving the SME. We then discuss signatures in several special limits.

A. Conventional mergers

In order to search for Lorentz violation in chirp signals produced by binary systems, we first need a realistic description of the expected wave without Lorentz violation. This section provides a brief discussion of conventional binary mergers and establishes the basic structure needed to construct gravitational-wave signals with Lorentz violation. For a review of the underlying conventional physics see, for example, Refs. [50, 51].

Starting in the time domain, we imagine an asymptotically flat frame centered on the merger. We orient the frame so that the binary revolves in the right-handed sense about the z axis. Far from the merger, the wave will be transverse to the propagation direction \hat{v} and the position vector $\vec{x} \approx r\hat{v}$. The conventional gravitational radiation is then completely described by either of the complex helicity components, since $h_{(+2)}(t) = h_{(-2)}^*(t)$ in the time domain, where $h_{\mu\nu}$ is real.

Conventional waves produced by binaries are dominated by their merger-frame $j = 2$, $m = \pm 2$ multipoles and are even under parity. This implies that the observed

wave takes the generic form

$$h_{(+2)}(t) = \mathcal{U}(t) {}_{-2}Y_{22}(\hat{v}) + \mathcal{U}^*(t) {}_{-2}Y_{2(-2)}(\hat{v}). \quad (29)$$

The wave is then completely characterized by a single complex scalar function $\mathcal{U}(t)$.

While the exact form of $\mathcal{U}(t)$ can only be found by considering the detailed physics of the merger, some general features can be ascertained. For example, splitting $\mathcal{U}(t)$ into an amplitude and a phase, $\mathcal{U}(t) = \mathcal{A}(t)e^{-i\Psi(t)}$, we expect both the phase $\Psi(t)$ and its rate of change to increase monotonically with time. To see this, we write $h_{(+2)}$ in terms of the spherical-coordinate angles θ and ϕ for the direction vector \hat{v} :

$$h_{(+2)}(t) = \sqrt{\frac{5}{4\pi}} (\mathcal{U}e^{2i\phi} \cos^4 \frac{\theta}{2} + \mathcal{U}^*e^{-2i\phi} \sin^4 \frac{\theta}{2}). \quad (30)$$

We then note that \mathcal{U} only contributes through the combination $\mathcal{U}e^{2i\phi} = \mathcal{A}e^{i(2\phi - \Psi)}$, so wavefronts satisfy $2\phi = \Psi + (\text{constant})$. Since we assume right-handed rotations about the z axis, we expect the azimuthal angle ϕ of a wavefront at a fixed distance from the merger to increase with time, so the phase function Ψ increases monotonically with time. Also, since the rotation of the binary accelerates as it inspirals, we expect a positive instantaneous oscillation frequency $\Omega(t) = \partial_t \Psi(t)$ that increases with time. We also note that the wave frequency Ω is twice the wavefront rotation rate, as expected in a binary system.

The frequency-domain version of Eq. (29) is more amenable to studies of Lorentz violation. Taking the fourier transform, we get

$$h_{(+2)}(f) = u(f) {}_{-2}Y_{22}(\hat{v}) + u^*(-f) {}_{-2}Y_{2(-2)}(\hat{v}), \quad (31)$$

where $u(f) = \int dt \mathcal{U}(t)e^{i2\pi ft}$, for $2\pi f = \omega$. The $u(f)$ function completely characterizes the wave in the frequency domain. The negative-helicity component can be found using $h_{(-2)}(f) = h_{(+2)}^*(-f)$. We also split the frequency-domain function

$$u(f) = A(f)e^{i\psi(f)} \quad (32)$$

into an amplitude and a phase.

The connection between the time- and frequency-domains can be studied through a stationary-phase approximation. For a fixed frequency f , the fourier transform $u(f) = \int dt \mathcal{A}(t)e^{i(2\pi ft - \Psi)}$ is dominated by times t_f that are extrema of the phase. These times are solutions to the equation $2\pi f = \Omega(t_f)$. Since the instantaneous frequency $\Omega(t)$ is positive, extrema only exist for positive frequencies, and we can assume that negative frequencies play an insignificant role in $u(f)$. The negative frequencies do affect the signal through $u^*(-f)$ in Eq. (31), however. Since Ω increases with time, we can in principle invert the relationship between f and t_f , so t_f is a single-valued function of f . Then the usual stationary-phase approximation gives $A(f) \approx \sqrt{2\pi/\partial_t^2 \Psi(t_f)} \mathcal{A}(t_f)$ and $\psi(f) \approx 2\pi ft_f - \Psi(t_f) - \frac{\pi}{4}$.

Applying the stationary-phase approximation to the inverse fourier transform yields similar relations. It implies that the dominant frequency f_t at time t is a solution of $2\pi t = \partial_f \psi(f_t)$. Again, since f_t and t are expected to rise together, we can assume $\partial_f^2 \psi(f_t)$ is positive. We then arrive at two key characteristics of the frequency-domain function $u(f) = A(f)e^{i\psi(f)}$. To a good approximation, we can assume that $u(f)$ is nonzero for positive frequencies only and that the phase function $\psi(f)$ is convex.

As a chirp progresses, it transitions from an inspiral to a merger, followed by the ringdown. Each stage is subject to different physics and gives different contributions to $A(f)$ and $\psi(f)$. For example, early in the inspiral the ‘‘newtonian’’ approximation is valid [52], which results in

$$\begin{aligned}\psi(f) &\approx 2\pi f t_0 + \psi_0 + \frac{3}{27\pi^{5/3}} \eta^{-1} (Tf)^{-5/3}, \\ A(f) &\approx C r^{-1} T^2 \eta^{1/2} (Tf)^{-7/6},\end{aligned}\quad (33)$$

where C is a constant, r is the distance from the source, t_0 determines the time origin, and ψ_0 is a phase constant. The important features of the chirp depend on the total mass $M = M_1 + M_2$ and mass ratio $\eta = M_1 M_2 / M^2$. Here we define the chirp time constant $T = G_N(1+z)M$, which gives the characteristic time scale. We incorporate the source redshift z to account for cosmological expansion.

The expressions in Eq. (33) provide a simple approximation that should hold at low frequencies. At higher frequencies, corresponding to later times, the approximation is expected to fail. More accurate descriptions at all frequencies can be achieved through a combination of higher-order post-newtonian corrections [51] and numerical relativity [53]. Analytic templates can be constructed to approximate the late-stage physics. These generally have a phase function of the form

$$\psi(f) = 2\pi f t_0 + \psi_0 + \sum_n (Tf)^{n/3} \psi_n, \quad (34)$$

where the ψ_n are constants. The amplitude $A(f)$ may also be modified. For example, Ref. [54] assumes an $A(f)$ that is proportional to $f^{-7/6}$ over inspiral frequencies, is proportional $f^{-2/3}$ for the merger, and decays as a lorentzian at higher ringdown frequencies. Their phase includes terms with $n = -5, -3, -2, -1, 1, 2$. All parameters are treated as functions of the mass ratio η and fit to results from post-newtonian and numerical relativity. The spins of the two bodies can also be incorporated in the templates [55].

B. Signatures of Lorentz violation

The choice of reference frame is important when testing Lorentz invariance since the coefficients for Lorentz violation are different in different frames. By convention, Lorentz tests report results using a Sun-centered celestial equatorial frame [22, 56]. The direction of propagation \hat{v}

has Sun-frame polar angle $\theta = \text{dec.} + 90^\circ$ and Sun-frame azimuthal angle $\phi = \text{r.a.} \pm 180^\circ$, in terms of the declination and right ascension of the source. The standard Sun-frame linear polarizations $h_{(+)}$ and $h_{(\times)}$ are related to the helicity components through Eq. (23). The axes of the $h_{(+)}$ polarization align with the celestial cardinal directions, while the axes for $h_{(\times)}$ polarization are along the intercardinal directions.

Equation (31) gives the predicted form for the Lorentz-invariant helicity components in the merger frame. Before we determine the effects of Lorentz violation, we first transform this result to the Sun frame. This is done by passively rotating Eq. (31) using the rotation operator $R = e^{i\alpha_z J_z} e^{i\alpha_y J_y} e^{i\alpha'_z J_z}$, where α_y , α_z , and α'_z are Euler angles relating the two frames. The rotation acting on the spherical harmonics gives $R_s Y_{jm} = \sum_{m'} D_{m'm}^{(j)}(-\alpha_z, -\alpha_y, -\alpha'_z) Y_{jm'}$, where $D_{m'm}^{(j)}$ are the Wigner rotation matrices. The Sun-frame Lorentz-invariant wave can then be written as

$$h_{(\pm 2)}^{\text{LI}}(f) = u(f) \mathcal{Y}_{(\pm 2)} + u^*(-f) \mathcal{Y}_{(\mp 2)}^*, \quad (35)$$

where it is convenient to define the direction-dependent factors

$$\begin{aligned}\mathcal{Y}_{(\pm 2)} &= \sum_m D_{m2}^{(2)}(-\alpha_z, -\alpha_y, 0)_{\mp 2} Y_{2m}(\theta, \phi) \\ &= \sum_m d_{m2}^{(2)}(-\alpha_y) e^{i\alpha_z m} Y_{2m}(\theta, \phi).\end{aligned}\quad (36)$$

The $d_{mm'}^{(j)}$ in the last line are little Wigner matrices.

The $\mathcal{Y}_{(\pm 2)}$ factors have helicity ± 2 and account for the location (θ, ϕ) and orientation (α_y, α_z) of the source in the Sun-centered frame. While the general rotation depends on the three Euler angles, the α'_z angle corresponds to a rotation about the merger-frame z axis. This is equivalent to a change in phase and can be absorbed into the phase constant ψ_0 . We may therefore take $\alpha'_z = 0$, leaving four angles to characterize the location and orientation of the binary in the Sun frame. Note that the $\mathcal{Y}_{(\pm 2)}$ also completely determine the polarization content in the conventional limit.

Restricting attention to positive f and using Eq. (22), the helicity components with Lorentz violation are

$$\begin{aligned}h_{(\pm 2)} &= u e^{i\delta} ((\cos \beta \mp i \cos \vartheta \sin \beta) \mathcal{Y}_{(\pm 2)} \\ &\quad - i e^{\mp i \varphi} \sin \vartheta \sin \beta \mathcal{Y}_{(\mp 2)}) .\end{aligned}\quad (37)$$

The negative-frequency parts can be found using the identity $h_{(\pm 2)}(f) = h_{(\mp 2)}^*(-f)$. In the linear basis, the positive-frequency parts become

$$\begin{aligned}h_{(+)} &= u e^{i\delta} ((\cos \beta - i \cos \varphi \sin \vartheta \sin \beta) \mathcal{Y}_{(+)} \\ &\quad - (\cos \vartheta + i \sin \varphi \sin \vartheta) \sin \beta \mathcal{Y}_{(\times)}) , \\ h_{(\times)} &= u e^{i\delta} ((\cos \beta + i \cos \varphi \sin \vartheta \sin \beta) \mathcal{Y}_{(\times)} \\ &\quad + (\cos \vartheta - i \sin \varphi \sin \vartheta) \sin \beta \mathcal{Y}_{(+)}),\end{aligned}\quad (38)$$

where $\mathcal{Y}_{(+)}$ and $\mathcal{Y}_{(\times)}$ are direction factors for linear polarizations and are related to helicity-basis factors through

$\mathcal{Y}_{(\pm 2)} = \mathcal{Y}_{(+)} \mp i\mathcal{Y}_{(\times)}$. The linear components both obey the conjugation rule $h_{(+,\times)}(f) = h_{(+,\times)}^*(-f)$, which implies the time-domain $h_{(+,\times)}(t)$ are real, as expected.

The signal generated in a given detector depends on its orientation relative to the Sun-centered frame at the time of the observation. The gravitational strain for a detector can be written as

$$\begin{aligned} h_{(D)} &= F_{(+)}h_{(+)} + F_{(\times)}h_{(\times)} \\ &= \frac{1}{2}F_{(+2)}^*h_{(+2)} + \frac{1}{2}F_{(-2)}^*h_{(-2)}. \end{aligned} \quad (39)$$

Assuming arms of equal length, the linear-basis antenna pattern functions are

$$\begin{aligned} F_{(+)} &= \frac{1}{2}(C_{\theta 1}^2 - C_{\phi 1}^2 - C_{\theta 2}^2 + C_{\phi 2}^2), \\ F_{(\times)} &= C_{\theta 1}C_{\phi 1} - C_{\theta 2}C_{\phi 2} \end{aligned} \quad (40)$$

where $C_{ak} = \hat{e}_a \cdot \hat{l}_k$ are the direction cosines between the Sun-frame \hat{e}_θ and \hat{e}_ϕ vectors and the arms of the detector, which point along unit vectors \hat{l}_1 and \hat{l}_2 . Assuming the \hat{l}_k vectors are horizontal, the cosines are

$$\begin{aligned} C_{\theta k} &= \cos(\phi - \alpha) \cos \theta \cos \chi \cos \xi_k + \sin \theta \sin \chi \cos \xi_k \\ &\quad + \sin(\phi - \alpha) \cos \theta \sin \xi_k, \\ C_{\phi k} &= \cos(\phi - \alpha) \sin \xi_k - \sin(\phi - \alpha) \cos \chi \cos \xi_k, \end{aligned} \quad (41)$$

where θ and ϕ are the Sun-frame propagation angles, χ is the colatitude of the detector, α is the right ascension of the laboratory zenith at the time of the detection, and ξ_k is the angle between \hat{l}_k and local south measured to the east. The helicity-basis pattern functions are given by $F_{(\pm 2)} = F_{(+)} \mp iF_{(\times)}$.

Using either the helicity components (37) or linear components (38), we find that the theoretical positive-frequency strain with Lorentz violation takes the simple form

$$h_{(D)} = A e^{i(\psi+\delta)} (\mathcal{F}^0 \cos \beta - i\vec{\mathcal{F}} \cdot \hat{\zeta} \sin \beta), \quad (42)$$

where

$$\hat{\zeta} = (\sin \vartheta \cos \varphi, \sin \vartheta \sin \varphi, \cos \vartheta) \quad (43)$$

is the Stokes rotation axis discussed in the Appendix. It is the normalized Stokes vector for the faster eigenmode and depends on the birefringence angles ϑ and φ defined in Eq. (15). The negative-frequency strain can be found using $h_{(D)}(f) = h_{(D)}^*(-f)$, ensuring that the time-domain strain is real.

We emphasize that Eq. (42) gives the leading-order theoretical strain signal for any realistic extension of linearized gravity, including all possible Lorentz-breaking and Lorentz-invariant modifications.

The unconventional effects in a given event are completely determined by the common phase δ , the birefringent phase β , and the ϑ and φ angles. The conventional degrees of freedom are those in the chirp amplitude $A(f)$

and phase $\psi(f)$ functions and in the Stokes-like parameters

$$\begin{aligned} \mathcal{F}^0 &= \frac{1}{2}(F_{(+2)}^*\mathcal{Y}_{(+2)} + F_{(-2)}^*\mathcal{Y}_{(-2)}), \\ \mathcal{F}^1 &= \frac{1}{2}(F_{(-2)}^*\mathcal{Y}_{(+2)} + F_{(+2)}^*\mathcal{Y}_{(-2)}), \\ \mathcal{F}^2 &= \frac{i}{2}(F_{(-2)}^*\mathcal{Y}_{(+2)} - F_{(+2)}^*\mathcal{Y}_{(-2)}), \\ \mathcal{F}^3 &= \frac{1}{2}(F_{(+2)}^*\mathcal{Y}_{(+2)} - F_{(-2)}^*\mathcal{Y}_{(-2)}). \end{aligned} \quad (44)$$

These complex factors represent a distillation of all the usual directional degrees of freedom.

The strain in the Lorentz-invariant case is $h_{(D)}^{\text{LI}} = \mathcal{F}^0 A e^{i\psi}$. In this limit, the incident polarization depends on the location and orientation of the source relative to the Earth but is the same for all frequencies. The conventional direction factor \mathcal{F}^0 accounts for the polarization of the incident wave and its alignment relative to the arms of the detector.

In Lorentz-violating cases with birefringence, different frequencies can have different polarizations, which gives additional f dependence characterized by the terms in brackets in Eq. (42). While nonbirefringent Lorentz violation affects the phase of the signal, birefringence can alter both the phase and the amplitude. The changes in amplitude can be isolated by considering the spectral density

$$\begin{aligned} |h_{(D)}|^2 &= A^2 (|\mathcal{F}^0|^2 \cos^2 \beta + |\vec{\mathcal{F}} \cdot \hat{\zeta}|^2 \sin^2 \beta \\ &\quad + \text{Im}(\mathcal{F}^{0*} \vec{\mathcal{F}} \cdot \hat{\zeta}) \sin 2\beta). \end{aligned} \quad (45)$$

Deviations from the expected spectral density $|\mathcal{F}^0|^2 A^2$ provide a generic signature of birefringence due to Lorentz violation.

C. Special cases

Equation (42) provides a general framework for searches Lorentz violation in chirp signals. While the SME describes an endless variety of possible Lorentz violations, experimental limitations likely preclude a broad search. It is therefore useful to focus on the three main classes of violations controlled by the three different coefficient combinations in Eq. (11). We again consider each case in turn.

Nonbirefringent violations. Setting all but the $k_{(I)jm}^{(d)}$ coefficients to zero yields the nonbirefringent limit. In this limit, the strain becomes

$$h_{(D)} = \mathcal{F}^0 A e^{i(\psi+\delta)}. \quad (46)$$

This simply adds the Lorentz-violating phase $\delta = (2\pi f)^{d-3} \tau \zeta^{(d)0}$ to the conventional phase function ψ . The modifications exist for even $d \geq 4$, but dispersion results only when $d \geq 6$. Figure 1 shows an example of dispersion in the strain signal for $d = 6$ Lorentz violations. A single point source can constrain one direction-

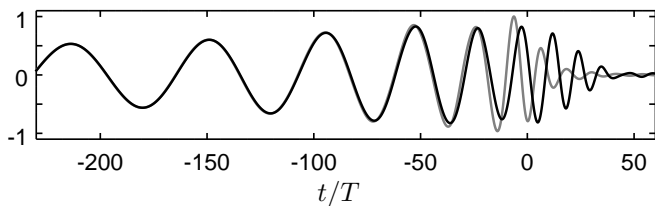


FIG. 1: Time-domain strain for nonbirefringent dispersion with $\tau\zeta^{(6)0} = 20T^3$ (black) and the Lorentz-invariant limit (gray). The Lorentz-invariant strain is generated using the amplitude and phase functions in Ref. [54] with mass ratio $\eta = \frac{1}{4}$.

dependent coefficient combination $\zeta^{(d)0}$, for fixed d . Measurements from multiple sources at different locations on the sky could be combined to limit the entire $k_{(I)jm}^{(d)}$ coefficient space.

A single source can, however, constrain the isotropic limit. At each d , there is one isotropic coefficient $k_{(I)00}^{(d)}$. Setting all other coefficients to zero yields a simple one-parameter special case with Lorentz-violating phase

$$\delta_{\text{iso}} = \frac{1}{\sqrt{4\pi}}(2\pi f)^{d-3} \tau k_{(I)00}^{(d)}. \quad (47)$$

This produces polarization- and direction-independent dispersion. Isotropic dispersion of the form $\omega^2 = |\vec{p}|^2 + A|\vec{p}|^\alpha$ has been considered [14]. This formalism maps to SME parameters through $\alpha = d - 2$ and $A = -\sqrt{1/\pi}k_{(I)00}^{(d)}$. Note that this implies that α is an even positive integer. Other values of α may occur in gauge-breaking theories or in non-field-theoretic descriptions of gravity, but both of these possibilities likely produce additional effects beyond simple dispersion. Odd α values do appear in the CPT-odd birefringent case discussed below. However, dispersion in that case is accompanied by changes in polarization.

CPT-odd birefringence. Taking nonzero $k_{(V)jm}^{(d)}$ coefficients gives the CPT-odd birefringent case. The result can be written in term of the phase $\delta\psi = (2\pi f)^{d-3}\tau\zeta_{(0)}^{(d)}$, for odd $d \geq 5$. The positive-frequency strain reduces to

$$h_{(D)} = A e^{i\psi} (\mathcal{F}^0 \cos \delta\psi - i\mathcal{F}^3 \sin \delta\psi), \quad (48)$$

and the spectral density becomes

$$|h_{(D)}|^2 = A^2 (|\mathcal{F}^0|^2 \cos^2 \delta\psi + |\mathcal{F}^3|^2 \sin^2 \delta\psi + \text{Im}(\mathcal{F}^{0*}\mathcal{F}^3) \sin 2\delta\psi). \quad (49)$$

Figure 2 shows an example of the theoretical strain from $d = 5$ CPT-odd birefringence. As in the nonbirefringent case, multiple sources at different locations on the sky are required to fully constrain the $k_{(V)jm}^{(d)}$ coefficient space for fixed d . This case also contains an isotropic limit, where

$$\delta\psi_{\text{iso}} = \frac{1}{\sqrt{4\pi}}(2\pi f)^{d-3}\tau k_{(V)00}^{(d)}. \quad (50)$$

A single source can fully constrain this simple special case.

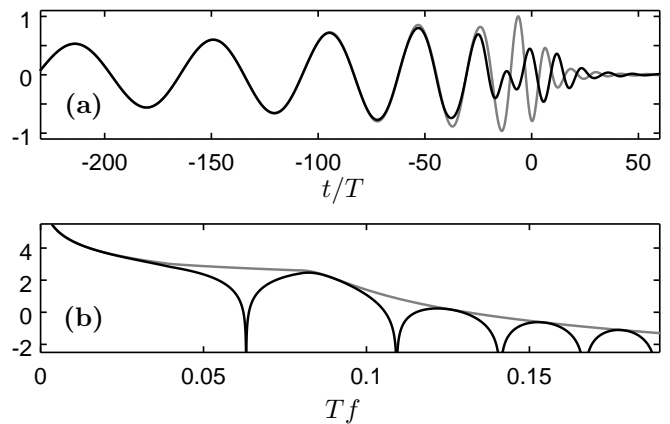


FIG. 2: (a) Time-domain strain and (b) base-10 logarithm of the spectral density for CPT-odd birefringence with $\tau\zeta_{(0)}^{(5)} = 10T^2$ (black). The Lorentz-invariant limit (gray) is generated using the phase and amplitudes from Ref. [54] with mass ratio $\eta = \frac{1}{4}$. The merger is positioned so that the incident wave is linearly polarized in the Lorentz-invariant limit, and the detector arms are aligned to maximize the conventional sensitivity.

CPT-even birefringence. For the CPT-even birefringent case, we take $k_{(E)jm}^{(d)}$ and $k_{(B)jm}^{(d)}$ coefficients to be nonzero. For fixed d , the strain is then given by Eq. (42), with $\delta = 0$, birefringent phase

$$\beta = (2\pi f)^{d-3}\tau |\zeta_{(+4)}^{(d)}|, \quad (51)$$

and

$$\vec{\mathcal{F}} \cdot \hat{\zeta} = \mathcal{F}^1 \cos \varphi + \mathcal{F}^2 \sin \varphi. \quad (52)$$

Using this direction factor in Eq. (45) gives the spectral density. The effects are therefore governed by the magnitude and phase of the coefficient combination $\zeta_{(+4)}^{(d)}$. No isotropic limit exists in this case. This is because the ± 4 -helicity $\zeta_{(\pm 4)}^{(d)}$ combinations couple the circular polarizations $h_{(\pm 2)}$, giving a change of ± 4 in helicity. Only scalar helicity-zero functions contain isotropic components, so violations of this type are necessarily anisotropic.

In both birefringent cases, the unlikely possibility exists that the observed gravitational wave is produced in one of the propagating eigenmodes. For the CPT-odd case, the eigenmodes are circularly polarized, implying that the Earth would need to lie on the z axis of the merger frame. The wave then maintains a fixed polarization, and the direction factors obey $\mathcal{F}^3 = \pm\mathcal{F}^0$. For the CPT-even case, the eigenmodes are linearly polarized, which means the Earth lies in the x - y plane of the merger frame, and the plane is aligned with a polarization axis of one of the eigenmodes. In this scenario, the direction factor satisfies $\vec{\mathcal{F}} \cdot \hat{\zeta} = \mathcal{F}^0$ for the fast mode and $\vec{\mathcal{F}} \cdot \hat{\zeta} = -\mathcal{F}^0$ for the slow mode. In both the CPT-odd and CPT-even cases, the polarization would be unaffected and there would be no sign of Lorentz violation

in the spectral density. However, the birefringent phase β produces dispersion and therefore still results in a deformed strain.

IV. SUMMARY AND DISCUSSION

In this paper, we derive and study signals for Lorentz violation in gravitational waves. We work in the linearized-gravity limit of the SME and consider all possible violations that preserve the usual gauge invariance. The violations involve $d - 2$ spacetime derivatives of the metric perturbation $h_{\mu\nu}$, where d is the mass dimension of the corresponding operator in the action, in natural units.

Leading-order plane-wave solutions are found in Sec. II. Lorentz violation results in two propagating modes with conventional leading-order polarizations. The modes can propagate at different frequency-dependent phase velocities, resulting in both dispersion and birefringence. While the effects depend on the propagation direction in general, one isotropic coefficient for Lorentz violation exists at each dimension d that gives direction-independent modifications. Equation (22) gives the effects of Lorentz violation on the circular-polarization components of a wave after propagating an astrophysical distance in terms of its Lorentz-invariant limit. Equation (24) gives the effects for the linear polarizations.

Signals of Lorentz violation in waves from coalescing binaries are derived in Section III. The key result is the detector-specific theoretical strain given in Eq. (42). While the emphasis of this paper is Lorentz violation, Eq. (42) describes in general the leading-order effects of any extension of linearized gravity, including all possible Lorentz-violating and Lorentz-invariant terms.

The theoretical chirp signal involves a number of unknown parameters that can only be determined through observation. The wave depends on the total binary mass M , the mass ratio η , and the redshift z . The spins of the objects may also play a role. There are two angles θ and ϕ that specify the location of the binary relative to the Earth. Two more angles α_y and α_z characterize its orientation.

Lorentz violation introduces a frequency-dependent common phase δ , which produces dispersion but no birefringence. It also results in a frequency-dependent birefringent phase β that gives both dispersion and birefringence. Birefringence produces changes in the polarization of the wave, which also depends on two angles ϑ and φ that determine the polarizations of the propagating eigenmodes. For a given source with propagation direction \hat{v} , all the Lorentz-violating parameters can be written in terms \hat{v} -dependent combinations of spherical coefficients for Lorentz violation using Eq. (11).

While the formalism developed here can be used to search for general Lorentz violations, forming a complete picture of a merger is challenging even in the usual case, due in part to the large number of degrees of freedom.

The task can be simplified by focusing on one of three limiting cases: nonbirefringent violations, CPT-odd birefringent violations, and CPT-even birefringent violations.

Nonbirefringent dispersion results from the $k_{(I)jm}^{(d)}$ coefficients for Lorentz violation. Dispersion deforms chirp waveforms by adding unconventional frequency dependence $\sim f^{d-3}$ to the phase. A single source can be used to limit the direction-dependent coefficient combination $\zeta^{(d)0}$ in Eq. (11) for $d = 6, 8, \dots$. Results from multiple sources at different locations on the sky could be combined to constrain the $k_{(I)jm}^{(d)}$ spherical coefficients for Lorentz violation for fixed dimension d .

While birefringent Lorentz violation comes with dispersion, a key signature differentiating it from the nonbirefringent case is a change a polarization that evolves as the wave propagates. The conventional case is expected to give a frequency-independent polarization, so a polarization that changes with frequency is an indicator for birefringent Lorentz violation.

While a single detector measures a single polarization component, a wave's polarization can in principle be reconstructed by combining the strain data from multiple detectors. Alternatively, signs of birefringence can be found in the spectral density. The spectral density of the strain is insensitive to the phase of incident wave and is therefore insensitive to dispersion. Changes in polarization due to birefringence distort a detectors response to a wave, affecting the strain amplitude. As a result, the spectral density is highly sensitive to frequency dependence in the polarization. The general predicted spectral density with Lorentz violation is given in Eq. (45). A deviation for the expected power law during the inspiral could be a signal of birefringence, for example.

CPT-odd and CPT-even birefringence each produce distinctive changes in the polarization. The $k_{(V)jm}^{(d)}$ coefficients give CPT-odd birefringence, which leads to a simple frequency-dependent rotation of the polarization about the propagation direction. The result is a change in the polarization angle but no change in the degree of linear or circular polarization. CPT-even birefringence stems from the $k_{(E)jm}^{(d)}$ and $k_{(B)jm}^{(d)}$ coefficients for Lorentz violation. The effects in the CPT-even case are more complicated, giving a change in the polarization angle and the degrees of linear and circular polarization.

Because the effects of Lorentz violation depend on the direction of propagation and the polarization, some waves may experience minimal defects even if Lorentz violation is significant in general. This leads to a potential selection bias that is common in other astrophysical tests. Dispersion and birefringence may distort a gravitational wave to the point where it is no longer recognizable as a potential chirp event. The detected waves may be those that happen to propagate in particular directions and have particular polarizations that produce very little change. This possibility can be ruled out experimentally by constraining the underlying coefficients for Lorentz violation through observations of multiple sources at dif-

ferent points on the sky and with different polarizations.

The precision at which Lorentz violation can be tested in a gravitational wave is largely determined by the effective propagation time τ and the chirp time constant T . The effects of Lorentz violation may be significant when the phase in Eq. (19) is of order one. Frequencies up to $\sim 1/T$ contribute to the chirp, so gravitational waves are expected to test combinations of coefficients for Lorentz violation at levels approaching $\sim T^{d-3}/\tau$. Assuming propagation distances on the order of a Gpc and a total mass of around fifty solar masses, this gives an approximate sensitivity at the level of $\sim 10^{-16}$ m to $d = 5$ coefficients and $\sim 10^{-11}$ m² to $d = 6$ coefficients.

At present, few gravitational-wave bounds exist on the spherical coefficients for Lorentz violation. Estimated limits on birefringence in GW150914 have been used to bound one combination of $d = 5$ CPT-odd $k_{(V)jm}^{(5)}$ coefficients at the level of 10^{-14} m and one combination of $d = 6$ CPT-even $k_{(E)jm}^{(6)}$ and $k_{(B)jm}^{(6)}$ coefficients at the level of 10^{-8} m² [12]. More sophisticated analyses will likely achieve sensitivities orders of magnitude beyond these bounds.

The best constraints on $k_{(I)jm}^{(6)}$ coefficients come from the absence of gravitational Čerenkov radiation in high-energy cosmic rays [21]. Lorentz violation in gravity can lead to subluminal wave speeds. High-energy particles traveling faster than gravity will radiate gravitational waves, losing energy. Observations of high-energy cosmic rays place stringent limits on the coefficients for Lorentz violation responsible for the changes in velocity. The high energies involved mean Lorentz invariance is tested at much higher frequencies, giving sensitivities that are many orders of magnitude beyond what can be achieved through observations of low-frequency mergers. However, Čerenkov studies generally make a number of simplifying assumptions concerning Lorentz violation in the cosmic-ray particles and their interactions with gravity, assumptions that may not hold in nature. By contrast, dispersion and birefringence provide clean signatures of Lorentz violation in pure gravity, completely independent of violations in other sectors.

Tests of short-range gravity have also placed constraints on $d = 6$ Lorentz violations [30]. Binary-merger observations are expected to give sensitivities to $d = 6$ violations that are several orders of magnitude better than short-range tests. Due to the long wavelengths of the gravitational waves and the sub-millimeter reach of the laboratory tests, short-range gravity experiments will likely achieve better sensitivities to higher- d violations. Note, however, that these tests should be viewed as complementary since gravitational waves provide access to the “vacuum” coefficients in Table I, while short-range experiments are sensitive to a different set of “Newton” coefficients $k_{jm}^{N(d)}$. Each of these sets of coefficients are different combinations of the underlying coefficients for Lorentz violation in Eq. (2), so the two classes of experiment test fundamentally different forms of Lorentz

violation.

Acknowledgments

This work was supported in part by the United States National Science Foundation under grant number PHY-1819412.

APPENDIX: STOKES PARAMETERS

As with electromagnetic radiation, one can define gravitational Stokes parameters that characterize the power associated with different polarizations. They also provide a simple picture for the effects of birefringence. While birefringence generally produces complicated changes in the polarization of a wave, the effects can be understood as a simple rotation of the Stokes parameters [22].

While gauge-invariant extensions of general relativity can in principle give up to 6 polarizations, resulting in 36 gravitational Stokes parameters [57], the limit considered in this work produces two propagating modes with conventional leading-order polarizations. For positive frequencies, we define four real gravitational Stokes parameters

$$\begin{aligned} S^0 &= |h_{(+)}|^2 + |h_{(\times)}|^2 = \frac{1}{2}(|h_{(+2)}|^2 + |h_{(-2)}|^2) , \\ S^1 &= |h_{(+)}|^2 - |h_{(\times)}|^2 = \text{Re}(h_{(+2)}^* h_{(-2)}) , \\ S^2 &= 2 \text{Re}(h_{(+)}^* h_{(\times)}) = \text{Im}(h_{(+2)}^* h_{(-2)}) , \\ S^3 &= 2 \text{Im}(h_{(+)}^* h_{(\times)}) = \frac{1}{2}(|h_{(+2)}|^2 - |h_{(-2)}|^2) . \end{aligned} \quad (53)$$

The Stokes parameters obey $(S^0)^2 = \vec{S}^2$, where $\vec{S} = (S^1, S^2, S^3)$ is the Stokes vector. The Stokes vector can also be written in terms of ± 4 -helicity components $S_{(\pm 4)} = S^1 \mp iS^2$ and a 0-helicity component $S_{(0)} = S^3$.

Some understanding of the Stokes parameters can be gained by parameterizing an arbitrary polarization using the form

$$h_{(\pm 2)} = a \left(\cos \frac{\chi}{2} \pm \sin \frac{\chi}{2} \right) e^{\mp i\zeta/2} , \quad (54)$$

where $-\frac{\pi}{2} \leq \chi \leq \frac{\pi}{2}$ and $0 \leq \zeta < 2\pi$. In the linear basis, we can write this as

$$\begin{pmatrix} h_{(+)} \\ h_{(\times)} \end{pmatrix} = a \begin{pmatrix} \cos \frac{\zeta}{2} & -\sin \frac{\zeta}{2} \\ \sin \frac{\zeta}{2} & \cos \frac{\zeta}{2} \end{pmatrix} \begin{pmatrix} \cos \frac{\chi}{2} \\ i \sin \frac{\chi}{2} \end{pmatrix} . \quad (55)$$

This gives general elliptical polarization along rotated axes $\hat{e}_1 = \cos \frac{\zeta}{4} \hat{e}_\theta + \sin \frac{\zeta}{4} \hat{e}_\phi$ and $\hat{e}_2 = \cos \frac{\zeta}{4} \hat{e}_\phi - \sin \frac{\zeta}{4} \hat{e}_\theta$, implying that $\frac{\zeta}{4}$ is the linear polarization angle. The angle χ determines the degree of circular polarization, with $\chi = 0$ for linear, $\chi = \frac{\pi}{2}$ for right-handed circular, and $\chi = -\frac{\pi}{2}$ for left-handed circular polarizations.

In terms of ζ and χ , the Stokes parameters are

$$S^0 = |a|^2 , \quad \vec{S} = S^0 (\cos \chi \cos \zeta, \cos \chi \sin \zeta, \sin \chi) . \quad (56)$$

Each Stokes vector \vec{S} defines a unique point on a sphere of radius S^0 analogous to the Poincaré sphere from optics. Every point on the sphere represents a unique polarization. Points in the S^1 - S^2 plane are the linear polarizations, with $h_{(+)}$ on the positive S^1 axis and $h_{(\times)}$ on the negative S^1 axis. The upper hemisphere, with $S^3 > 0$, contains all right-handed elliptical polarizations, and the lower hemisphere gives left-handed elliptical polarizations. The poles correspond to the two circular polarizations. In general, orthogonal polarizations point to opposite points on the sphere. The degree of linear polarization is $\cos \chi$, and $\sin \chi$ gives the degree of circular polarization.

Assuming Eq. (31), the Lorentz-invariant Stokes parameters for a merger are

$$\begin{aligned} S_{\text{LI}}^0 &= \frac{1}{2}|u|^2(\cos^8 \frac{\theta}{2} + \sin^8 \frac{\theta}{2}), \\ S_{\text{LI}}^1 &= |u|^2 \sin^4 \frac{\theta}{2} \cos^4 \frac{\theta}{2}, \\ S_{\text{LI}}^2 &= 0, \\ S_{\text{LI}}^3 &= \frac{1}{2}|u|^2(\cos^8 \frac{\theta}{2} - \sin^8 \frac{\theta}{2}), \end{aligned} \quad (57)$$

in the merger frame. Note that this only depends on the merger-frame polar angle θ . This shows that we get right-handed circular polarization along the $+z$ merger axis and left-handed circular polarization along the $-z$ axis. Waves traveling in the x - y plane are linearly polarized. All linear and elliptical polarizations have a polarization angle of $\frac{\zeta}{4} = 0$. In the Sun frame, the Stokes parameters are $S_{\text{LI}}^\mu = |u|^2 S_y^\mu$, where S_y^μ are the Stokes parameters constructed from the direction factors in Eq. (36).

The Lorentz-violating parameters in Eq. (10) can be thought of as conveniently normalized Stokes parameters for the birefringent eigenmodes. The vector

$$\vec{\zeta} = \left(\frac{1}{2}(\zeta_{(+4)} + \zeta_{(-4)}), \frac{i}{2}(\zeta_{(+4)} - \zeta_{(-4)}), \zeta_{(0)} \right) \quad (58)$$

points in the direction of the Stokes vector for the faster eigenmode and opposite the vector for the slower mode. Note, however, that $(\zeta^0)^2 \neq \zeta^2$.

Changes in polarization due to birefringence will cause the Stokes vector \vec{S} of a wave to evolve as it propagates. Only waves with \vec{S} along $\vec{\zeta}$, corresponding to one of the eigenmodes, will remain unaltered. To find the effects for other polarizations, we define the orthonormal Stokes basis

$$\begin{aligned} \hat{\zeta} &= \vec{\zeta}/|\vec{\zeta}| = (\sin \vartheta \cos \varphi, \sin \vartheta \sin \varphi, \cos \vartheta), \\ \hat{\vartheta} &= (\cos \vartheta \cos \varphi, \cos \vartheta \sin \varphi, -\sin \vartheta), \\ \hat{\varphi} &= (-\sin \varphi, \cos \varphi, 0), \end{aligned} \quad (59)$$

in terms of the birefringence angles ϑ and φ . Expanding an arbitrary Stokes vectors in this basis, $\vec{S} = S^\zeta \hat{\zeta} + S^\vartheta \hat{\vartheta} + S^\varphi \hat{\varphi}$, we arrive at a set of Stokes parameters associated with the eigenmodes,

$$\begin{aligned} S^\zeta &= \frac{1}{2}(|h_{(f)}|^2 - |h_{(s)}|^2), \\ S^\vartheta &= \text{Re}(h_{(f)}^* h_{(s)}), \quad S^\varphi = \text{Im}(h_{(f)}^* h_{(s)}). \end{aligned} \quad (60)$$

An eigenmode differs from its Lorentz-invariant limit by a phase, $h_{(f,s)} = e^{i\delta \mp i\beta} h_{(f,s)}^{\text{LI}}$, giving

$$\begin{aligned} S^\zeta &= S_{\text{LI}}^\zeta, \\ S^\vartheta &= \cos(2\beta) S_{\text{LI}}^\vartheta - \sin(2\beta) S_{\text{LI}}^\varphi, \\ S^\varphi &= \cos(2\beta) S_{\text{LI}}^\varphi + \sin(2\beta) S_{\text{LI}}^\vartheta. \end{aligned} \quad (61)$$

This shows that the Stokes vector with Lorentz violation \vec{S} can be obtained from the Stokes vector without Lorentz violation \vec{S}_{LI} by rotating \vec{S}_{LI} about the axis $\hat{\zeta}$ by angle 2β , which is the change in relative phase due to birefringence.

In the CPT-odd case, where $\vartheta = 0$ or $\vartheta = \pi$, the rotation axis $\hat{\zeta}$ points to one of the poles of the Poincaré sphere. Birefringence causes a rotation about the S^3 axis by $\delta\zeta = \pm 2\beta$, changing the linear polarization angle by $\pm\beta/2$.

For the CPT-even birefringence, where $\vartheta = \pi/2$, the rotation axis $\hat{\zeta}$ lies in the S^1 - S^2 plane at an angle φ from the S^1 axis. Unless \vec{S}_{LI} happens to align with $\hat{\zeta}$, the Stokes vector rotates on a cone centered around $\hat{\zeta}$. This causes changes in both the ζ and χ polarization angles. The linear polarization angle changes, as do the degree of linear polarization and degree of circular polarization.

The Stokes parameters can also be used to track the evolution of the polarization as it propagates from the source to the observer. The infinitesimal change in phase $d\psi_\pm = d\psi_0 + \omega(-\zeta^0 \pm |\vec{\zeta}|)dl$ changes the eigenmodes by $dh_{(f,s)} = -id\psi_\pm h_{(f,s)}$. The result is an infinitesimal rotation of the Stokes parameters about $\hat{\zeta}$. The rotation can be written

$$\frac{d\vec{S}}{dl} = 2\omega\vec{\zeta} \times \vec{S}, \quad (62)$$

giving right-handed rotations of \vec{S} about $\hat{\zeta}$ at a rate of $2\omega|\vec{\zeta}|$.

-
- [1] B.P. Abbott *et al.*, LIGO and Virgo Collaborations, Phys. Rev. Lett. **116**, 061102 (2016).
 [2] B.P. Abbott *et al.*, LIGO and Virgo Collaborations, Phys. Rev. Lett. **116**, 241103 (2016).

- [3] B.P. Abbott *et al.*, LIGO and Virgo Collaborations, Phys. Rev. Lett. **118**, 221101 (2017).
 [4] B.P. Abbott *et al.*, LIGO and Virgo Collaborations, Astrophys. J. **851**, L35 (2017).

- [5] B.P. Abbott *et al.*, LIGO and Virgo Collaborations, *Phys. Rev. Lett.* **119**, 141101 (2017).
- [6] B.P. Abbott *et al.*, LIGO and Virgo Collaborations, *Phys. Rev. Lett.* **119**, 161101 (2017).
- [7] For reviews see, e.g., R. Bluhm, *Lect. Notes Phys.* **702**, 191 (2006); S. Liberati, *Class. Quant. Grav.* **30**, 133001 (2013); J.D. Tasson, *Rep. Prog. Phys.* **77**, 062901 (2014); A. Hees *et al.*, *Universe* **2**, 30 (2016).
- [8] V.A. Kostelecký and N. Russell, *Data Tables for Lorentz and CPT Violation*, 2019 edition, arXiv:0801.0287v12.
- [9] V.A. Kostelecký and R. Potting, *Phys. Rev. D* **51**, 3923 (1995); D. Colladay and V.A. Kostelecký, *Phys. Rev. D* **55**, 6760 (1997); *Phys. Rev. D* **58**, 116002 (1998).
- [10] V.A. Kostelecký, *Phys. Rev. D* **69**, 105009 (2004).
- [11] V.A. Kostelecký and S. Samuel, *Phys. Rev. D* **39**, 683 (1989); V.A. Kostelecký and R. Potting, *Nucl. Phys. B* **359**, 545 (1991).
- [12] V.A. Kostelecký and M. Mewes, *Phys. Lett. B* **757**, 510 (2016).
- [13] B.P. Abbott *et al.*, LIGO and Virgo Collaborations, arXiv:1811.00364; arXiv:1903.04467.
- [14] S. Mirshekari, N. Yunes, and C.M. Will, *Phys. Rev. D* **85**, 024041 (2012).
- [15] D. Hansen, N. Yunes, and K. Yagi, *Phys. Rev. D* **91**, 082003 (2015); A. Samajdar and K.G. Arun, *Phys. Rev. D* **96**, 104027 (2017); H.A.S. Costa, P.R.S. Carvalho, and I.G. da Paz, *Int. J. Mod. Phys. D* **28**, 1950028 (2018); T.P. Sotiriou, *Phys. Rev. Lett.* **120**, 041104 (2018); A. Nishizawa, *Phys. Rev. D* **97**, 104037 (2018); S.C. Yang *et al.*, arXiv:1812.04350.
- [16] N. Yunes, K. Yagi, and F. Pretorius, *Phys. Rev. D* **94**, 084002 (2016).
- [17] S. Wang, arXiv:1712.06072.
- [18] A. Nishizawa, *Phys. Rev. D* **93**, 124036 (2016); E. Passos *et al.*, *Phys. Lett. B* **772**, 870 (2017).
- [19] B.P. Abbott *et al.*, LIGO, Virgo, Fermi, and INTEGRAL Collaborations, *Astrophys. J.* **848**, L13 (2017).
- [20] C.M. Caves, *Annals Phys.* **125**, 35 (1980); G.D. Moore and A.E. Nelson, *JHEP* **0109**, 023 (2001); J.W. Elliott, G.D. Moore, and H. Stoica, *JHEP* **0508**, 066 (2005); R. Kimura and K. Yamamoto, *JCAP* **1207**, 050 (2012); M. De Laurentis, S. Capozziello, and G. Basini, *Mod. Phys. Lett. A* **27**, 1250136 (2012); S. Kiyota and K. Yamamoto, *Phys. Rev. D* **92**, 104036 (2015).
- [21] V.A. Kostelecký and J.D. Tasson, *Phys. Lett. B* **749**, 551 (2015); J. Tasson, *Symmetry* **8**, 111 (2016); M. Schreck, *Symmetry* **10**, 424 (2018).
- [22] V.A. Kostelecký and M. Mewes, *Phys. Rev. D* **80**, 015020 (2009).
- [23] V.A. Kostelecký and M. Mewes, *Phys. Rev. D* **85**, 096005 (2012); *Phys. Rev. D* **88**, 096006 (2013); V.A. Kostelecký and Z. Li, *Phys. Rev. D* **99**, 056016 (2019).
- [24] H. Müller *et al.*, *Phys. Rev. Lett.* **100**, 031101 (2008); K.-Y. Chung *et al.*, *Phys. Rev. D* **80**, 016002 (2009); M.A. Hohensee *et al.*, *Phys. Rev. Lett.* **106**, 151102 (2011).
- [25] N.A. Flowers, C. Goodge, and J.D. Tasson, *Phys. Rev. Lett.* **119**, 201101 (2017); C.-G. Shao *et al.*, *Phys. Rev. D* **97**, 024019 (2018).
- [26] J.B.R. Battat, J.F. Chandler, and C.W. Stubbs, *Phys. Rev. Lett.* **99**, 241103 (2007); A. Bourgoïn *et al.*, *Phys. Rev. Lett.* **117**, 241301 (2016); A. Bourgoïn *et al.*, *Phys. Rev. Lett.* **119**, 201102 (2017).
- [27] L. Iorio, *Class. Quant. Grav.* **29**, 175007 (2012); A. Hees *et al.*, *Phys. Rev. D* **92**, 064049 (2015); Q.G. Bailey and D. Havert, *Phys. Rev. D* **96**, 064035 (2017).
- [28] Q.G. Bailey, R.D. Everett, and J.M. Overduin, *Phys. Rev. D* **88**, 102001 (2013).
- [29] L. Shao, *Phys. Rev. Lett.* **112**, 111103 (2014); *Phys. Rev. D* **90**, 122009 (2014); R.J. Jennings, J.D. Tasson, and S. Yang, *Phys. Rev. D* **92**, 125028 (2015); L. Shao and Q.G. Bailey, *Phys. Rev. D* **98**, 084049 (2018); L. Shao and Q.G. Bailey, *Phys. Rev. D* **99**, 084017 (2019).
- [30] Q.G. Bailey, V.A. Kostelecký, and R. Xu, *Phys. Rev. D* **91**, 022006 (2015); J.C. Long and V.A. Kostelecký, *Phys. Rev. D* **91**, 092003 (2015); C.-G. Shao *et al.*, *Phys. Rev. D* **91**, 102007 (2015); C.-G. Shao *et al.*, *Phys. Rev. Lett.* **117**, 071102 (2016).
- [31] C.G. Shao *et al.*, *Phys. Rev. D* **94**, 104061 (2016); Y.F. Chen, Y.J. Tan, and C.G. Shao, *Symmetry* **9**, 219 (2017); C.-G. Shao *et al.*, *Phys. Rev. Lett.* **122**, 011102 (2019).
- [32] J.D. Tasson, *Phys. Rev. D* **86**, 124021 (2012).
- [33] M.A. Hohensee, H. Müller, and R.B. Wiringa, *Phys. Rev. Lett.* **111**, 151102 (2013).
- [34] Q.G. Bailey, *Phys. Rev. D* **80**, 044004 (2009); C. Le Poncin-Lafitte, A. Hees, and S. Lambert, *Phys. Rev. D* **94**, 125030 (2016).
- [35] V.A. Kostelecký and J.D. Tasson, *Phys. Rev. D* **83**, 016013 (2011).
- [36] Q.G. Bailey and V.A. Kostelecký, *Phys. Rev. D* **74**, 045001 (2006).
- [37] R. Bluhm and V.A. Kostelecký, *Phys. Rev. D* **71**, 065008 (2005); R. Bluhm, S.H. Fung, and V.A. Kostelecký, *Phys. Rev. D* **77**, 065020 (2008); M.D. Seifert, *Phys. Rev. D* **79**, 124012 (2009); *Phys. Rev. D* **81**, 065010 (2010); *Symmetry* **10**, 490 (2018); B. Altschul, Q.G. Bailey, and V.A. Kostelecký, *Phys. Rev. D* **81**, 065028 (2010); R. Bluhm, *Phys. Rev. D* **91**, 065034 (2015); *Symmetry* **9**, 230 (2017); R. Bluhm and A. Sehic, *Phys. Rev. D* **94**, 104034 (2016); J. Foster, V.A. Kostelecký, and R. Xu, *Phys. Rev. D* **95**, 084033 (2017); Q.G. Bailey and C.D. Lane, *Symmetry* **10**, 480 (2018).
- [38] V.A. Kostelecký and J.D. Tasson, *Phys. Rev. Lett.* **102**, 010402 (2009); Q.G. Bailey, *Phys. Rev. D* **82**, 065012 (2010); *Phys. Rev. D* **94**, 065029 (2016); R. Tso and Q.G. Bailey, *Phys. Rev. D* **84**, 085025 (2011); Y. Bonder, *Phys. Rev. D* **91**, 125002 (2015); M. Schreck, *Class. Quant. Grav.* **34**, 135009 (2017); Y. Bonder and G. Leon, *Phys. Rev. D* **96**, 044036 (2017); Y. Bonder and C. Corral, *Symmetry* **10**, 433 (2018).
- [39] V.A. Kostelecký and M. Mewes, *Phys. Lett. B* **779**, 136 (2018).
- [40] V.A. Kostelecký and M. Mewes, *Phys. Lett. B* **766**, 137 (2017).
- [41] A.F. Ferrari *et al.*, *Phys. Lett. B* **652**, 174 (2007); R.V. Maluf *et al.*, *Phys. Rev. D* **90**, 025007 (2014); L.H.C. Borges and D. Dalmazi, *Phys. Rev. D* **99**, 024040 (2019).
- [42] V. Vasileiou *et al.*, *Phys. Rev. D* **87**, 122001 (2013); F. Kislak and H. Krawczynski, *Phys. Rev. D* **92**, 045016 (2015); J.J. Wei *et al.*, *Astrophys. J.* **842**, 115 (2017).
- [43] V.A. Kostelecký and M. Mewes, *Astrophys. J.* **689**, L1 (2008).
- [44] A.S. Friedman *et al.*, *Phys. Rev. D* **99**, 035045 (2019).
- [45] V.A. Kostelecký and M. Mewes, *Phys. Rev. Lett.* **87**, 251304 (2001); *Phys. Rev. D* **66**, 056005 (2002); *Phys. Rev. Lett.* **97**, 140401 (2006); *Phys. Rev. Lett.* **99**, 011601 (2007); *Phys. Rev. Lett.* **110**, 201601 (2013); E.Y.S. Wu *et al.*, QUaD Collaboration, *Phys. Rev. Lett.* **102**, 161302 (2009); E. Komatsu *et al.*, WMAP Collab-

- oration, *Astrophys. J. Suppl.* **180**, 330 (2009); *Astrophys. J. Suppl.* **192**, 18 (2011); Z. Xiao and B.Q. Ma, *Phys. Rev. D* **80**, 116005 (2009); Q. Exirifard, *Phys. Lett. B* **699**, 1 (2011); F. Kislak and H. Krawczynski, *Phys. Rev. D* **95**, 083013 (2017); F. Kislak, *Symmetry* **10**, 596 (2018); L. Pogosian *et al.*, arXiv:1904.07855.
- [46] R. Lehnert and R. Potting, *Phys. Rev. Lett.* **93**, 110402 (2004); *Phys. Rev. D* **70**, 125010 (2004); *Phys. Rev. D* **70**, 129906(E) (2004); C. Kaufhold and F.R. Klinkhamer, *Nucl. Phys. B* **734**, 1 (2006); *Phys. Rev. D* **76**, 025024 (2007); B. Altschul, *Phys. Rev. D* **90**, 021701(R) (2014); *Phys. Rev. D* **92**, 125016 (2015); *Symmetry* **9**, 250 (2017); K. Schober and B. Altschul, *Phys. Rev. D* **92**, 125016 (2015); D. Colladay, P. McDonald, and R. Potting, *Phys. Rev. D* **93**, 125007 (2016).
- [47] B. Altschul, *Phys. Rev. Lett.* **98**, 041603 (2007); *Phys. Rev. D* **75**, 105003 (2007); *Phys. Rev. D* **93**, 105007 (2016); F.R. Klinkhamer and M. Schreck, *Phys. Rev. D* **78**, 085026 (2008); J.S. Diaz, V.A. Kostelecký, and M. Mewes, *Phys. Rev. D* **89**, 043005 (2014); J.S. Diaz and F.R. Klinkhamer, *Phys. Rev. D* **92**, 025007 (2015); H. Martínez-Huerta and A. Pérez-Lorenzana, *Phys. Rev. D* **95**, 063001 (2017); M. Schreck, *Phys. Rev. D* **96**, 095026 (2017); K. Astapov, D. Kirpichnikov and P. Satunin, arXiv:1903.08464.
- [48] M. Isi and A.J. Weinstein, arXiv:1710.03794; B.P. Abbott *et al.*, LIGO and Virgo Collaborations, *Phys. Rev. Lett.* **120**, 201102 (2018).
- [49] B.P. Abbott *et al.*, *Astrophys. J.* **848**, L12 (2017).
- [50] C.M. Will *Living Rev. Rel.* **17**, 4 (2014).
- [51] L. Blanchet *Living Rev. Rel.* **17**, 2 (2014).
- [52] See, e.g., Sec. 36.6 of C.W. Misner, K.S. Thorne, and J.A. Wheeler, *Gravitation*, W. H. Freeman, San Francisco, CA, 1973.
- [53] M. Campanelli *et al.*, *Phys. Rev. Lett.* **96**, 111101 (2006); J.G. Baker *et al.*, *Phys. Rev. Lett.* **96**, 111102 (2006).
- [54] P. Ajith *et al.*, *Phys. Rev. D* **77**, 104017 (2008); *Phys. Rev. D* **79**, 129901(E) (2009).
- [55] P. Ajith *et al.*, *Phys. Rev. Lett.* **106**, 241101 (2011).
- [56] R. Bluhm *et al.*, *Phys. Rev. Lett.* **88**, 090801 (2002); *Phys. Rev. D* **68**, 125008 (2003).
- [57] A.M. Anile and R.A. Breuer, *Astrophys. J.* **189**, 38 (1974).